

Evaluation of cloud phase retrieval methods for SEVIRI onboard Meteosat-8 using ground-based lidar and cloud radar data

Erwin L.A. Wolters*, Robert A. Roebeling, and Arnout J. Feijt

November 5, 2007

⁰All authors: Royal Netherlands Meteorological Institute, De Bilt, The Netherlands.

*Corresponding author, E-mail: wolterse@knmi.nl

Abstract

Three cloud phase determination algorithms (Moderate Resolution Imaging Spectroradiometer (MODIS)-like thermal infrared cloud phase method, Satellite Application Facility on Climate Monitoring (CM-SAF) method, and an International Satellite Cloud Climatology Project (ISCCP)-like method) from passive satellite imagers are explored to assess their suitability for climate monitoring purposes in midlatitude coastal climate zones. Using one year (May 2004-April 2005) of data from the Spinning Enhanced Visible and Infrared Imager (SEVIRI) onboard the first Meteosat Second Generation satellite (Meteosat-8), retrievals of the methods are compared to collocated and synchronized ground-based cloud phase retrievals obtained from cloud radar and lidar observations at Cabauw, the Netherlands. Three aspects of the satellite retrievals are evaluated: 1) Instantaneous cloud phase retrievals, 2) monthly averaged water and ice cloud occurrence frequency, and 3) diurnal cycle of cloud phase for May-August 2004. For the instantaneous cases, all methods show very small bias for thick water and ice cloud retrievals ($\sim 5\%$). The ISCCP-like method has a larger bias for pure water clouds ($\sim 10\%$), which is likely due to the 260 K threshold leading to misdetection of water clouds existing at lower temperatures. For the monthly averaged water and ice cloud occurrence, the CM-SAF method is best capable of reproducing the annual cycle, mainly for the water cloud occurrence frequency, for which an almost constant positive bias of $\sim 8\%$ was found. The ISCCP- and MODIS-like methods have more problems to detect the annual cycle, especially during the winter months. The difference in annual cycle detection between the three methods is most probably related to the use of visible/near-infrared reflectances which enable a more direct observation of cloud phase. The diurnal cycle in cloud phase is well reproduced by all methods. The MODIS-like method reproduces the diurnal cycle best, with correlations of 0.89 and 0.86 for water and ice cloud occurrence frequency, respectively.

1. Introduction

The interaction between clouds and radiation is of great importance to the Earth's surface energy balance. Clouds reflect and absorb solar radiation and emit and absorb terrestrial radiation. The cloud-radiation interaction is of a complex nature and is dependent upon properties such as cloud particle size, cloud temperature, cloud phase, water vapor and aerosol abundance, and surface reflectivity. Accurate detection of cloud phase is important because water and ice clouds influence the surface energy balance differently. Water clouds reflect shortwave irradiance, while ice clouds absorb and emit outgoing terrestrial radiation back to the Earth's surface. Cloud phase determination can be regarded as the next step after cloud masking to retrieve cloud properties from satellite measurements.

During the past few decades, several approaches to infer cloud phase from satellite imagery have been developed. Based on the type of spectral information used, these methods can be divided into three groups. The first group uses thermal infrared radiances, the second group utilizes visible and near-infrared reflectances, whereas the third group uses a combination of visible, near-infrared, and thermal infrared radiances.

The advantage of using only thermal infrared radiances is the capability of obtaining cloud phase information during both daytime and nighttime, which enables detection of the diurnal cycle of cloud phase. In contrast, visible and near-infrared methods can only be applied during daytime. Since outgoing surface radiance significantly contributes to the radiance measured by a satellite instrument, thermally based cloud phase retrievals are sensitive to errors when detecting optically thin and broken clouds. In addition, brightness temperature thresholding affects cloud phase by assuming a sudden transition from water to ice clouds below a certain temperature

threshold, whereas in reality this transition depends on e.g. cloud dynamics and the cloud condensation nuclei concentration. As a result, cloud-top temperature indicates rather than observes cloud phase. Arking and Childs (1985) obtained information on cloud thermodynamic phase based primarily from 3.7- and 10.8- μm channel radiances of the Advanced Very High Resolution Radiometer (AVHRR) onboard the National Oceanographic and Atmospheric Administration (NOAA) satellite. Strabala et al. (1994) developed a trispectral method to determine cloud phase using radiances of the 8.5-, 11- and 12- μm bands of the Moderate-Resolution Imaging Spectroradiometer (MODIS), which was adopted for operational use within the MODIS scientific cloud datasets (Platnick et al. 2003). Rossow and Schiffer (1999) defined a threshold for the cloud-top temperature derived from 10.8- μm brightness temperature to discriminate water from ice clouds within the International Satellite Cloud Climatology Project (ISCCP).

The methods of the second group are based on visible and near-infrared reflectances, which directly depend on the optical properties of liquid and solid cloud particles. At visible wavelengths, reflectance is primarily a function of cloud optical thickness, whereas at longer wavelengths (such as the cloud particle absorption bands around 1.6 μm) reflectance is dominated by particle size (Nakajima and King 1990). Hansen and Pollack (1970) used the differences between visible and near-infrared reflectances to derive cloud particle phase and size. Pilewskie and Twomey (1987) performed ground-based reflectance measurements between 0.63 and 1.9 μm to derive cloud phase at convective cloud edges. Knap et al. (2002) developed a method using 1.64- and 1.70- μm reflectances from the Airborne Visible and Infrared Imaging Spectrometer (AVIRIS) to generate accurate cloud phase retrievals over ocean surfaces.

The methods of the third group utilize combinations of visible, near-infrared, and thermal infrared radiances. The strength of combining visible with thermal infrared information is that

the quality of the retrievals can be improved through the combination of different tests, while a disadvantage is the limitation to daytime cloud scenes due to the usage of visible and near-infrared data. Baum et al. (2000) improved the trispectral thermal infrared method of Strabala et al. (1994) by adding 0.63-, 1.63- and 1.90- μm reflectances to increase the cloud phase retrieval accuracy for thin cirrus clouds. The cloud phase determination method used within the Satellite Application Facility on Climate Monitoring (CM-SAF) of the European Organization for the Exploration of Meteorological Satellites (EUMETSAT) combines 0.6- and 1.6- μm reflectance with an additional cloud-top temperature check for the retrieval of ice clouds.

Although good progress in our theoretical understanding of retrieving cloud phase information from passive imagers has been made, most validation efforts have been performed on a small number of cases. Little is known about the accuracy of the various cloud phase determination methods when applied to long-term datasets, which form the basis for climate monitoring applications, like ISCCP, CM-SAF, and the MODIS Atmosphere group.

Despite several ground-based measurement campaigns focusing on the radiative importance of supercooled water or mixed-phase clouds from ground-based measurements have been performed (Hogan et al. 2003; Turner et al. 2003; Turner 2005), little research has been done to explore the quality of water and ice phase retrievals. In this paper we investigate the suitability of three widely used satellite cloud phase retrieval methods for climate monitoring purposes in a midlatitude coastal climate, using data from the Spinning Enhanced Visible and Infrared Imager (SEVIRI) onboard the first Meteosat Second Generation satellite (Meteosat-8). All methods use multiple spectral channels. The methods investigated are: (i) a MODIS-like method using brightness temperature difference 8.7-10.8 μm combined with 10.8- μm brightness temperature, (ii) an ISCCP-like method using a cloud-top temperature of 260 K as threshold, and (iii) a combined

0.6/1.6 μm reflectance method with an additional cloud-top temperature check, which is used within the CM-SAF. Method (i) is part of the first group of methods, since only thermal infrared radiances are used, whereas (ii) and (iii) are part of the third group.

The accuracy of the satellite water and ice phase retrievals is assessed by comparing retrievals to ground-based cloud phase obtained from cloud radar and lidar using an algorithm described by Illingworth and Coauthors (2007). Firstly, the accuracy of the three methods is assessed for homogeneous water or ice cloud cases. Subsequently, it is investigated whether the methods are able to detect both the annual and diurnal cycle in liquid water and ice cloud occurrence as observed from the ground.

The paper is organized as follows. Section 2 describes the satellite cloud phase determination methods evaluated, as well as the method for retrieving cloud phase from ground-based lidar and cloud radar measurements. In section 3, satellite and surface data processing is presented. Validation results for the different satellite cloud phase determination methods are shown in section 4 and conclusions are drawn in section 5.

2. Cloud phase determination algorithms

2a. *Satellite algorithms*

i. *MODIS thermal infrared cloud phase determination method*

The MODIS bispectral infrared cloud phase algorithm is part of the MODIS Atmosphere Science Dataset (SDS), which is currently in its fifth reprocessing cycle (Collection 5, see for more information <http://modis.gsfc.nasa.gov/>). It uses the combination of 8.5-11.0 μm brightness tem-

perature difference (hereafter referenced as $BTD_{8.5-11}$) and 11.0- μm brightness temperature to determine cloud phase (Platnick et al. 2003). The method relies on the fact that for water and ice the absorption efficiency coefficients are nearly equal in the water vapor absorption region around 8 μm , while around 11 μm ice is a more efficient absorber than water and thus has a lower brightness temperature (see Figure 1). Strabala et al. (1994) showed that $BTD_{8.5-11}$ values around zero can be expected for clear sky scenes, whereas $BTD_{8.5-11}$ is positive and negative for ice and water clouds, respectively. Since SEVIRI has a spectral channel centered at 8.7 μm instead of 8.5 μm , the spectral difference between the two channels likely affects the brightness temperature difference. Due to less water vapor absorption in the SEVIRI 8.7 μm spectral band, the SEVIRI 8.7- μm brightness temperature is higher than the MODIS 8.5- μm brightness temperature. To account for this effect, all $BTD_{8.5-11}$ thresholds used by the MODIS group were adjusted for use on SEVIRI (see Table 1). Furthermore, errors in the conversion of the SEVIRI thermal infrared radiance to brightness temperature (EUMETSAT 2007) necessitated an additional correction to both the 8.7- and 10.8- μm brightness temperatures.

[Table 1 about here.]

The MODIS cloud phase determination method classifies cloud flagged pixels into four categories: water, ice, mixed phase, and undefined. Since this paper focuses on the quality of water and ice detection, undefined classifications were discarded from the dataset, while mixed phase classifications ($\sim 8\%$ of all cloud phase retrievals) were added to the ice category, because from visual image inspection of one month of MODIS images over Europe revealed that mixed phase is mainly retrieved from the (optically thin) edges of ice clouds.

[Figure 1 about here.]

ii. ISCPP-like cloud phase determination method

A widely used way to infer cloud phase information is by thresholding thermal infrared brightness temperatures. That is, a cloud flagged pixel having a brightness temperature lower than a certain threshold value is attributed to the ice phase. The water vapor saturation pressure difference in clouds between water and ice reaches its maximum near 261 K (Pruppacher and Klett 1997), which implies that below these temperatures ice particles are more easily formed than water particles.

For opaque clouds, the measured 10.8 μm brightness temperature can be regarded as the thermodynamic temperature from the uppermost part of the cloud, since the cloud emissivity, ε , approaches unity. Furthermore, absorption by water vapor in the atmospheric column above the cloud is negligible for the 10.8 μm spectral channel. For semi-transparent or broken cloud cases, the radiance emitted by the cloud is approximated as follows:

$$R_m = \varepsilon_\lambda R_{cl} + (1 - \varepsilon_\lambda) R_{sur}, \quad (1)$$

with R_m the radiance measured at 10.8 μm , R_{cl} the cloud radiance, ε_λ the cloud emissivity at wavelength λ , and R_{sur} the surface radiance, to be estimated from the near-surface temperature. From Equation (1) it follows that for semi-transparent and broken clouds the brightness temperature obtained from measured 10.8- μm radiance is not representative for the real cloud temperature, due to the contribution of the surface radiance.

In order to account for $\varepsilon_\lambda < 1$, the 10.8- μm radiance is corrected. The correction uses the cloud (absorption) optical thickness at 10.8 μm , $\tau_{10.8}$, which is related to the cloud (scattering) optical thickness at 0.6 μm , $\tau_{0.6}$, obtained directly from visible reflectance measurements:

$$\tau_{10.8} = \tau_{0.6} \frac{Q_{10.8}}{Q_{0.6}}, \quad (2)$$

with $Q_{10.8}$ and $Q_{0.6}$ the extinction efficiency factors at 10.8 and 0.6 μm , respectively. When neglecting thermal infrared scattering, the cloud emissivity at 10.8 μm , $\varepsilon_{10.8}$, can be calculated using $\tau_{10.8}$ (Minnis et al. 1998):

$$\varepsilon_{10.8} = 1 - \exp\left(-\frac{\tau_{10.8}}{\mu}\right), \quad (3)$$

with μ the cosine of the satellite viewing zenith angle. A consequence of using $\tau_{0.6}$ is that this correction can only be applied during daytime. A similar approach is utilized by ISCCP to obtain cloud phase for low and midlevel clouds, using 260 K as threshold temperature (Rossow and Schiffer 1999). Riédi et al. (2001) found a sharp transition from pure water to pure ice clouds at 240 K when they compared Polarization and Directionality of the Earth’s reflectances (POLDER) cloud phase retrievals to lidar and radar cloud top retrievals at the Atmospheric Radiation Measurement (ARM) site at Oklahoma (USA). It was suggested to change the temperature threshold used in ISCCP accordingly. These results were contradicted by Hogan et al. (2003), who found a more gradual decrease in (supercooled) water occurrence at temperatures from 268 K down to 238 K using ground-based lidar measurements at Chilbolton (United Kingdom).

iii. *CM-SAF cloud phase determination method*

This method was developed at the Royal Netherlands Meteorological Insitute (KNMI) as part of the Cloud Physical Properties algorithm (Jolivet and Feijt 2005; Roebeling et al. 2006a) within

the framework of the CM-SAF. The method uses differences in the water and ice absorption characteristics to discern water from ice clouds. At near-infrared wavelengths, ice particles absorb sunlight more efficiently than water particles and will thus have a lower reflectance. The retrieval of cloud phase is done iteratively by comparing observed satellite reflectances at 0.6 μm and 1.6 μm to lookup tables (LUTs) of Radiative Transfer Model (RTM) simulated reflectances. Water and ice are assigned to those cloudy pixels for which the measured 0.6- and 1.6- μm SEVIRI reflectances correspond to the respective simulated LUT reflectance. Cloud flagged pixels initially assigned as ice are labeled as water if the emissivity corrected cloud-top temperature exceeds 265 K.

The LUT reflectances are modeled using the Doubling Adding KNMI (DAK) RTM (De Haan et al. 1987; Stammes 2001), which calculates shortwave reflectance at the top of the atmosphere assuming plane parallel homogeneous clouds above a Lambertian surface. The phase function of water droplets is calculated using Mie theory for spherical particles assuming a Gamma size distribution (Hansen and Travis 1974) with an effective variance, v_{eff} , of 0.15 and effective radii ranging from 1-24 μm . Ray tracing is used to calculate the ice particle phase function for imperfect hexagonal crystals of type a ($r_{\text{eff}}=4.6 \mu\text{m}$), C1 ($r_{\text{eff}}=12.3 \mu\text{m}$), C2 ($r_{\text{eff}}=26.2 \mu\text{m}$), and C3 ($r_{\text{eff}}=51.4 \mu\text{m}$) of the Cirrus Optical Properties (COP) ice crystal library (Hess and Wiegner 1994). Surface albedo information is obtained from the MODIS white sky surface albedo product (Platnick et al. 2003).

A cross section of the DAK ice and water LUTs is shown in Figure 2. Solar zenith angle, θ_{\circ} , viewing zenith angle, θ , and azimuth difference angle, $\phi-\phi_{\circ}$, are chosen at 28°, 20°, and 100°, respectively. The upper part of Figure 2 represents cloud reflectances modeled for water particles with effective radii of 3-24 μm , whereas cloud reflectances for ice crystals of type a, C1, C2 and C3

are displayed in the lower part. Cloud optical thickness for the SEVIRI 0.6 μm spectral channel, hereinafter referenced as cloud optical thickness, $\tau_{0.6}$, and r_{eff} can be retrieved independently for $\tau_{0.6} > 4$, because their LUT contours intersect (nearly) orthogonally. Further, the plots show that the 0.6- and 1.6- μm reflectances of small ice crystals and large water droplets overlap for $\tau_{0.6} > \sim 4$. For these cases, the emissivity corrected cloud-top temperature with threshold value 265 K is used as a cloud phase indicator.

[Figure 2 about here.]

2b. *Cloud phase determination from ground-based measurements*

A method to determine cloud phase from lidar and cloud radar measurements described by Illingworth and Coauthors (2007) is applied to measurements of the CloudNET site of Cabauw (The Netherlands, 51.97°N, 4.93°E, see Figure 3 for its location). The algorithm simultaneously uses cloud radar vertical Doppler velocity, lidar attenuated backscatter profiles, and Numerical Weather Prediction (NWP) model temperature profiles.

[Figure 3 about here.]

Cloud radar measures both the reflectivity of (cloud) particles and the convolution of particle velocity and vertical air motion. The wavelength of cloud radar instruments is such that in most cases the size of cloud particles is much smaller than the wavelength of the incident beam, which means that the Rayleigh scattering regime applies. Within this regime, radar reflectivity (Z) is proportional to the second moment of particle mass. The cloud radar at Cabauw is operated at a frequency of 35 GHz ($\lambda=8.6$ mm) with a beamwidth of 0.36° and a vertical resolution of about

90 m. Due to its proportionality to particle mass, the cloud radar reflectivity signal is dominated by large cloud particles. Optically thin layers consisting of large ice crystals may show up as geometrically very thick layers in the cloud radar reflectivity signal. Furthermore, in case of heavy rain the signal becomes saturated due to the large reflectivity from rain droplets, which implies that no cloud property information can be derived from higher cloud levels.

Lidar is mostly used to identify the cloud base of liquid water clouds. For cloud optical thickness values lower than ~ 4 also the cloud top height can be detected with an accuracy of tens to hundreds of meters (Chepfer et al. 2000). The backscatter coefficient, β , is the amount of emitted photons scattered back to the lidar instrument by atmospheric particles, such as cloud droplets or aerosols. The attenuated backscatter coefficient, β' , which is usually reported, is the backscatter coefficient corrected for gaseous absorption. The majority of the lidar instruments operates from ultraviolet up to near-infrared wavelengths. At Cabauw, a 0.905 μm lidar with a vertical resolution of ~ 30 m is operated.

Determination of cloud phase is performed in three steps. First, the algorithm estimates the cloud melting layer height, taking the level where the NWP model wet-bulb temperature (T_w) equals 0°C . Subsequently, this estimate is refined using the cloud radar vertical Doppler velocity profile, since in general a large and sharp increase in the fall speed of cloud particles can be detected at the melting layer. It is noted here that the Doppler vertical velocity is only searched when the model wet-bulb temperature is between -5°C and $+5^\circ\text{C}$. If the melting layer is outside this temperature region the altitude of the melting layer height is assumed at levelCOT $T_w=0^\circ$ (Hogan, personal communication, 2007). However, the probability of the model wet-bulb temperatures being outside this region is very small. Mittermaier and Illingworth (2003) showed that for the Met Office Unified mesoscale model (UM) the obtained 0°C wet-bulb temperature level has a bias of

+15 m compared to radar obtained values for the t+0h to t+5h forecast, with an rms error of 147 m. Finally, if available, the attenuated lidar backscatter coefficient is evaluated to determine the presence of thin supercooled water layers within ice clouds. The method described above enables cloud phase determination for the vertical profile up to ~ 12 km with a vertical resolution of ~ 90 m.

The following output categories from the ground-based algorithm are considered: "cloud liquid droplets", "drizzle/rain & cloud droplets", "ice", "ice & supercooled droplets", "melting ice", and "melting ice & cloud droplets". For the comparison of satellite cloud phase retrievals with ground observed cloud phase, the above categories were binned into three new categories for each sampling period: the "cloud droplets" and "drizzle/rain & cloud droplets" categories were labeled as water, the "ice" and "melting ice" categories were labeled as ice, and "ice & supercooled droplets" and the "melting ice & cloud droplets" categories were labeled as mixed phase.

Note that simultaneously using active cloud radar and lidar provides information on the vertical geometrical extent of a cloud and its properties, while passive satellite radiometers are mainly sensitive to the optical thickness of a cloud. In particular, the sensitivity of cloud radar reflectivity to large cloud particles requires attention. If an ice cloud contains large particles, radar reflectivity is high due to the proportionality with particle mass. However, if the ice water content of the cloud is low, the extinction and hence the cloud optical thickness is low. Due to this low extinction, SEVIRI may not be capable of detecting ice clouds with relatively low ice water contents, which increases the likelihood of cloud phase misclassification when such a cloud overlays a water cloud. Moreover, it should be noted that the quality of the ground-based cloud phase observations is best when both cloud radar and lidar data are available. That is, when the lidar is unavailable or attenuated due to thick low level water clouds, higher levels cannot be searched for

supercooled water. Therefore these ground-based retrievals should be carefully interpreted when used for evaluation of satellite derived cloud phase.

3. Data and methods

3a. Satellite data analysis

All satellite algorithms were tested using one year (May 2004-April 2005) of data from SEVIRI. The SEVIRI instrument contains 12 spectral channels: one visible, three near-infrared, seven thermal infrared, and one high-resolution visible channel. For this study, the 0.6-, 1.6-, 8.7-, and 10.8- μm spectral channels were used.

SEVIRI daytime data was archived at a 15-minute resolution. The SEVIRI 0.6 and 1.6 μm reflectances were cross-calibrated with the corresponding reflectances from MODIS-Terra, which carries in-flight absolute calibration instruments with an expected uncertainty of about 2% for the visible channels (Doelling et al. 2004; Roebeling et al. 2006a).

The algorithm to separate cloud free from cloud contaminated and cloud filled pixels is based on the MODIS cloud detection algorithm (Platnick et al. 2003). This algorithm has been simplified and modified to make it applicable for SEVIRI (<http://www-loa.univ-lille1.fr/~riedi/>). The input to the SEVIRI cloud detection algorithm consists of normalized reflectances from the visible (0.6 μm and 0.8 μm) and near-infrared (1.6 μm) channels, whereas brightness temperatures are used from the thermal infrared channels (3.8, 8.7, 10.8 and 12.0 μm). In addition, the algorithm uses ancillary data on solar and viewing geometry and a land/sea map. There are spectral threshold and spatial coherence cloud detection tests that are different for land and ocean surfaces. The SEVIRI thresholds differ slightly from the MODIS thresholds because of differences

in instrument calibration, channel characteristics and spatial resolution between the instruments.

Cloud phase was determined for individual pixels using the methods introduced in Section 2a. For the ISCCP-like method, a temperature threshold of 260 K was used. R_{sur} (see Equation 1) was calculated by applying the Planck function, weighted for the SEVIRI 10.8- μm spectral band, to European Center for Midrange Weather Forecasts (ECMWF) 10-meter temperature. The 10-meter temperature was chosen because in cloudy situations the difference between 10-meter and surface skin temperature is small. Values for $Q_{10.8}$ and $Q_{0.6}$, used to convert $\tau_{0.6}$ into $\tau_{10.8}$, were obtained using a polynomial fit through values from Mie calculations for effective radii between 1 and 24 μm . Subsequently, the cloud-top temperature was obtained using Equations (1) and (3). For the CM-SAF method, retrievals were limited to $\theta_o \leq 72^\circ$. Although not consistent with the recommendation of Loeb and Coakley (1998) to only use 1D simulated cloud reflectance for $\theta_o < \sim 60^\circ$, it was chosen to exceed this limit to also include boreal winter observations in the dataset. Furthermore, cases in which the MODIS-like method retrieval was undefined were discarded for all methods.

3b. Ground-based data analysis

Ground-based cloud phase observations were recorded at a 15-second time resolution at Cabauw, The Netherlands. To account for the difference in observation techniques between satellite and ground-based instruments, the ground-based observations were collected over a 30-minute time window centered at the SEVIRI scanning time for Cabauw, being about 12 minutes past the slot time. Furthermore, to minimize broken cloud field effects or mismatch in cloud detection between satellite and ground-based instruments, only cases with cloud cover $>90\%$ within the 30-minute

time window were included.

The ground-based observations derive cloud phase at both a high temporal resolution and for an entire cloud profile rather than only for the cloud top. In addition, water clouds with a geometrical thickness of a few hundred meters are mostly optically thick, whereas ice clouds often have low optical thickness even when their geometrical thickness is large. Therefore criteria were developed to interpret each 30-minute time window into a single cloud phase value.

It was shown in section 2b that for each sampling period the six cloud phase categories as obtained from the algorithm of Illingworth and Coauthors (2007) were binned into a water, ice, and mixed phase category. For each of these three categories the thickness per sampling period (15 s) was calculated. Subsequently, the average thickness of the three categories within the 30-minute time window period was calculated. Finally, threshold values were set for the average ice, water, and mixed phase cloud thickness to attribute the time window period to a unique cloud phase. Table 2 presents the criteria that are used to interpret 30-minute averaged water, ice, and mixed phase cloud thickness (Δh_w , Δh_i , and Δh_m , respectively) in terms of a single cloud phase for the considered period. Cloud systems with $\Delta h_i < 600$ m and $(\Delta h_w/\Delta h_m) > 4$ were labeled as water cloud. Clouds with $\Delta h_i < 2500$ m were labeled as ice, whereas for $\Delta h_i < 2500$ m and $(\Delta h_w/\Delta h_m) < 4$ mixed phase was assigned.

[Table 2 about here.]

3c. Comparison of satellite to ground-based cloud phase observations

The comparison of the satellite retrievals to ground observed cloud phase was divided into three parts: (i) instantaneous water and ice cloud retrievals, (ii) monthly averages of water and ice cloud

occurrence frequency using a three-month moving window, and (iii) diurnal cycle of cloud phase. The latter was performed for May-August 2004 only, since the diurnal cycle of water and ice occurrence frequency can be distinguished best when convection prevails, as is mostly the case during the Western European summer months.

i. Instantaneous water and ice cloud retrievals

A first quality indication of the satellite cloud phase determination methods was achieved by comparing instantaneous water and ice retrievals to collocated retrievals from the ground-based algorithm. Hereinafter, 'collocated' is used to indicate both the spatial collocation and the synchronization of two measurements. To quantify the detection accuracy of satellite cloud phase retrievals for different ground observed cloud thicknesses, the ground ice cloud dataset was sorted into groups of cloud cases with the 30-minute averaged ice cloud thickness from >200 m to >5000 m. The water cloud cases were grouped into classes with ≤ 200 m to ≤ 2500 m of ice cloud overhead. For these instantaneous water and ice cases the bias in the satellite retrieved cloud phase was determined.

Satellite data was obtained from two pixels nearest to the Cabauw geolocation. Roebeling et al. (2006b) showed that the difference between simulated SEVIRI and ground-based LWP values has a minimum at a ground tracklength of ~ 4 km. Taking into account the westerly air-flow, which dominates the Western European climate, and the SEVIRI pixel size of $\sim 4 \times 7$ km at the Cabauw geolocation, the validation area comprises the Cabauw pixel and the pixel west of Cabauw.

From the one-year dataset, collocated cases (both spatially and temporally) with a ground-

based cloud cover >90% and labeled as either water or ice by both satellite and ground-based observations were selected. Subsequently, the collocated cases were compared. For both water and ice, the number of cases with satellite cloud phase retrievals being different from the ground observed value divided by the total number of collocated water (ice) cases indicates the bias for instantaneous water (ice) retrievals.

ii. Monthly liquid water and ice cloud occurrence frequency

To examine the accuracy of the various methods with respect to climate monitoring purposes, the monthly averaged water and ice cloud occurrence frequency, $\overline{\varphi}_m^p$ and $\overline{\varphi}_m^p$, defined as the ratio of clouds labeled as water or ice to the total observed clouds, was calculated. The superscript p is hereinafter used to generically denote water and ice. Using the criteria from Table 2, the daily water and ice cloud occurrence frequency were calculated first:

$$\varphi_d = \frac{n_d^p}{N_d}, \quad (4)$$

with n_d^p and N_d the number of observed water or ice clouds and total number of clouds at a day, respectively.

The monthly averaged occurrence frequency was calculated using a three-month moving window. Since the number of available collocated time slots changed significantly for each day, a weighting factor, w_d , was defined:

$$w_d = \frac{n_d}{\sum_{d=0}^n n_d}, \quad (5)$$

with n_d the number of collocated time slots at day d having a ground-based derived cloud cover $>90\%$ and at least one satellite validation pixel cloud flagged. For both the SEVIRI and ground-based data, the monthly averaged water and ice cloud occurrence frequency, $\overline{\varphi}_m^p$, was calculated as follows:

$$\overline{\varphi}_m^p = \frac{n_m^p}{N_m}, \quad (6)$$

with n_m^p being the number of observed water or ice clouds and N_m being the total observed clouds within the three-month moving window.

The main accuracy indicator is the monthly bias in water and ice cloud occurrence frequency, B_m^p :

$$B_m^p = \overline{\varphi}_{m,sat}^p - \overline{\varphi}_{m,sur}^p, \quad (7)$$

with suffixes m, sat and m, sur referring to the monthly satellite and surface derived water and ice cloud occurrence frequency, respectively. The weighted unbiased root-mean-square error, $URMSE$, is used as a precision measure and indicates the spread in the differences between daily satellite and ground observed water or ice cloud occurrence frequency after removing the monthly bias:

$$URMSE = \sqrt{\sum_{d=0}^n w_d (\varphi_{d,sat}^p - B_m^p - \varphi_{d,sur}^p)^2} \quad (8)$$

A second precision indicator of the satellite retrieved daily measurements is the linear correlation coefficient. To account for the different weights given to each day, the correlation was

calculated using the product of w_d and φ_d^p . The correlation coefficient for the water and ice cloud occurrence frequency is calculated as follows:

$$r = \frac{cov((\varphi_d^p w_d)_{sat}, (\varphi_d^p w_d)_{sfc})}{\sigma_{sfc}^p \sigma_{sat}^p} \quad (9)$$

A high correlation between the satellite and surface water or ice cloud occurrence frequency indicates a good skill of the satellite method.

iii. *Diurnal cycle of cloud phase*

To assess the methods' ability for detecting the diurnal cycle of cloud phase, a four-month period during the boreal summer (May-August 2004) was investigated. This period was chosen since in the Western European coastal climate region, in which Cabauw is located, cloud formation during the summer is mostly induced by convection and to a lesser degree by synoptic-scale systems. Therefore it is expected that as a result of enhanced convection during the afternoon, the ice cloud occurrence frequency increases accordingly.

All cases with ground-based observed cloud cover >90% were collected and binned into 15-minute observation time categories for the period 6:12-18:12 UTC (8:12-20:12 Central European Summer Time). For each bin the average water and ice occurrence frequency was calculated. Subsequently, the correlation coefficient between satellite and surface methods was calculated. The error in the obtained correlation was calculated using a bootstrap technique. This technique uses the actual dataset to construct synthetic datasets by randomly drawing values from the original data (Efron and Tibshirani 1993).

4. Results

4a. *Instantaneous cloud phase retrievals*

The satellite based cloud phase retrieval is expected to perform better with increasing (optical) thickness of the observed cloud layer. In order to test this hypothesis, the accuracies of the satellite based ice phase retrievals are determined for ground-based observed ice clouds with a geometrical thickness increasing from 200 m to 5000 m. It is likely that the bias for the satellite ice retrievals will decrease with increasing geometrical thickness of the ice clouds over the ground-based sites. The SEVIRI phase retrievals are insensitive to geometrically thin (subvisual) ice clouds ($\tau_{0.6} < 1$), for which the SEVIRI phase retrievals are rather influenced by the water cloud or surface underneath. This may result in the incorrect retrieval of the water phase.

Similarly, the accuracy of the satellite water phase retrievals is determined for ground observed water clouds with an increasing ice cloud thickness overhead. For the validation of water clouds, an increasing ice thickness implies that more ice over water is allowed before the ground-based observed cloud phase is switched from water to the mixed phase category. It is therefore expected that with an increasing ice over water thickness the number of satellite ice retrievals will increase, hence increasing the bias with the ground observed cloud phase.

Figure 4 presents results for the instantaneous satellite cloud phase retrievals for May 2004–April 2005. Results are obtained for ice clouds with an increasing geometrical thickness and for water clouds with an increasing ice geometrical thickness overhead. The results for water clouds are plotted in grey, while the results for ice clouds are plotted in black. Values on the x-axis indicate the maximum and minimum ice thickness for ground observed water and ice clouds, respectively. Please note that the datasets are not equal in size, since the water cloud dataset

comprises ground observed water clouds with ice clouds aloft and the ice cloud dataset contains ground observed ice clouds, which do not necessarily have water clouds below. From Figure 4 it can be seen that the satellite cloud phase retrieval methods show small bias when almost pure water clouds (with ≤ 200 m ice overhead) are observed from the surface, with values of 4%, 7%, and 10% for the CM-SAF, MODIS-like, and ISCCP-like methods, respectively. The relatively high value for the ISCCP-like method is probably connected to the usage of 260 K as threshold, which fails to detect water clouds that exist at lower temperatures. Hogan et al. (2003) showed that the supercooled water occurrence frequency decreases from 27% towards 0% at temperatures between 268 K and 238 K, using ground-based lidar observations at Chilbolton (United Kingdom). As the ground observed ice cloud thickness over water clouds increases, the bias increases for all methods. This increase indicates that the satellite methods tend to retrieve ice more often with increasing ground observed ice cloud thickness over water clouds. The MODIS- and ISCCP-like methods are slightly more sensitive to an increase of ice thickness than the CM-SAF method, which is seen from the larger increase in bias than CM-SAF between >500 m and >1500 m ice thickness. Once ground observed ice thickness exceeds 1500 m, all methods show a similar increase in bias.

[Figure 4 about here.]

The ice retrieval results show an opposite behavior when ground observed ice thickness increases. If ground observed clouds with average ice thickness >200 m are labeled as ice, bias for the satellite methods is 50-55%, due to the SEVIRI spectral channels not being able to detect very thin ice clouds. However, at increasing minimum ice thickness the bias decreases exponentially; for clouds with ice thickness >3500 m, the bias for the three methods diminishes to within 5%.

Above results indicate that all methods have good skill for instantaneous retrievals if only thick, homogeneous water and ice clouds are considered.

[Figure 5 about here.]

4b. Monthly liquid water and ice cloud occurrence frequency

The monthly averaged liquid water and ice cloud occurrence frequency is used to monitor the annual variations in cloud phase. Figure 5 shows the monthly averaged distribution between water, ice, and mixed phase clouds as derived from ground-based measurements using a three-month moving window. Water clouds overlaid by <600 m ice are still considered water; clouds with ice thickness >2500 m are labeled ice (see also Table 2). The remaining cases are labeled mixed phase. The ice cloud occurrence frequency peaks during the late summer, which could be related to convective activity mostly taking place in the Western European climate in these months. The maximum water cloud occurrence frequency is observed in November 2004, which is probably connected to more synoptical weather systems moving over the Cabauw site. The mixed phase cloud occurrence frequency gradually increases towards the winter months from 30% to $\sim 60\%$, which is likely due to more supercooled water clouds within the synoptic-scale systems. It was shown by Rauber and Tokay (1991) that supercooled water layers are most likely to occur in non-convective clouds. Corresponding results were reported by Naud et al. (2006), who found that glaciation in midlatitude storms occurs at lower temperatures for shallow clouds outside the frontal regions. Note that the number of observations, indicated by the grey histogram, is strongly skewed towards the summer months, which implies that occurrence frequencies obtained for the winter months are significantly less reliable.

[Figure 6 about here.]

The monthly water and ice cloud occurrence frequency for the satellite methods and the ground-based reference dataset are given in Figures 6a and 6d. The water and ice cloud occurrence frequency is shown in the left and right panel, respectively. Further, the monthly URMSE (see Equation 8) is presented in Figures 6b and 6e. It is mentioned that due to the limited visible channel information the number of observations is low during November 2004-January 2005 (see Figure 5). The ground observed water occurrence frequency decreases during the summer months, having a minimum in September 2004. The decline (increase) in water (ice) occurrence frequency is likely related to summer convection. Water occurrence increases towards the (boreal) winter months, which may be connected to dominating synoptic-scale weather systems in the Western European climate region.

All methods show very small bias ($<5\%$) throughout the summer months. Towards autumn and winter, both the ISCCP- and MODIS-like methods predict a lower water occurrence frequency than the ground-based observed value. For the ISCCP-like method, this underestimation could be related to differences in cloud dynamics between summer and winter (convectively versus synoptically induced clouds) and thus more water clouds existing at temperatures lower than the 260 K threshold (Raubert and Tokay 1991; Hogan et al. 2003). The CM-SAF method has a continuous positive bias of $\sim 8\%$ for almost the entire year. URMSE is small for all methods, with a slight increase towards the winter months. For the CM-SAF and ISCCP-like methods this could be related to unfavorable viewing geometries (large solar and viewing zenith angles), which affect the accuracy of simulated 0.6- and 1.6- μm reflectances and hence the precision of the cloud phase retrieval. The MODIS-like method mostly has a smaller URMSE (higher precision) than the CM-SAF and ISCCP-like methods.

The derived ice cloud occurrence frequency shows a similar pattern for the summer months. Towards winter, all methods have a decrease in both accuracy and precision, as seen by the increase in bias and URMSE. In December 2004, all methods overestimate the ground-based derived ice cloud occurrence frequency by $\sim 15\%$, together with an increase in URMSE from $\sim 2\%$ in September to 16% in December 2004. The increase in URMSE indicates a larger spread of the differences between daily satellite and ground-based derived ice cloud occurrence frequency, which is partly related to substantially less collocated observations compared to the summer months. The precision of the CM-SAF method significantly improves after December 2004, as the URMSE drops from 16% to $\sim 3\%$. This indicates that the precision of cloud phase determination using visible and near-infrared reflectance is largely influenced by the viewing geometry. For the ISCCP-like method, the overestimation of ice clouds during the winter coincides with an underestimation of water clouds, which suggests that 260 K is a too high temperature threshold to accurately estimate the monthly average of cloud phase during winter in a midlatitude climate. Except for the large positive bias from October-December 2004, the CM-SAF method is best capable of detecting the ground-based observed ice cloud occurrence frequency.

To assess the methods' ability for reproducing the ground-based observed annual cycle in cloud phase, Figures 6c and 6 show the monthly averaged water and ice cloud occurrence frequency normalized by its yearly average in the left and right panel, respectively. For water clouds, the CM-SAF method almost perfectly detects the monthly variability in occurrence frequency as observed by the ground-based algorithm, probably linked to the usage of 0.6 and $1.6\ \mu\text{m}$ reflectance which enables a more direct cloud phase observation than temperature thresholding methods. During autumn and winter, the ISCCP-like method reproduces the annual cycle in water cloud occurrence frequency less clearly, which can be seen in Figure 6c from November 2004

onwards. For ice clouds, all methods reproduce the monthly variability well during summer. In the winter months, this ability decreases, although the CM-SAF method approaches the ground observed ice cloud occurrence frequency again from January 2005 onwards.

[Figure 7 about here.]

Weighted correlation coefficients for the retrieved daily water and ice cloud occurrence frequencies are presented in Figure 7. All methods have a high correlation (>0.8) for the summer months and show a decrease during the winter months for both water and ice. Further, correlation between satellite methods and ground-based observations is higher for ice cloud than for water cloud occurrence frequency with almost similar correlation coefficients for all methods. Correlation coefficients are very high (>0.9) until December 2004, followed by a decrease to ~ 0.75 during the winter. For the water cloud occurrence frequency, the ISCCP-like method shows a sharper drop in correlation than the CM-SAF and MODIS-like methods. Note that from December 2004 to January 2005 the number of observations is very low, which makes the correlations more susceptible to outliers. Table 3 presents the weighted correlation coefficients for the entire dataset together with values obtained from a bootstrap technique (Efron and Tibshirani 1993), which gives information on the reliability of the obtained correlations.

[Table 3 about here.]

4c. Diurnal cycle of cloud phase

Figure 8 shows the ground-based and satellite derived diurnal cycle of water (left panel) and ice occurrence frequency (right panel) for May-August 2004. Results are shown for one-hour

binned observations, while calculations of the correlation between satellite and ground observed water and ice cloud occurrence were performed using 15-minute binned data. The grey histogram denotes the number of collected observations for each hour from 6:12-18:12 UTC (8:12-20:12 Central European Summer Time, CEST).

[Figure 8 about here.]

During the morning and early afternoon, the ground-based observed water occurrence frequency is approximately constant ($\sim 40\%$), while the ice cloud occurrence frequency shows a small increase. The water cloud occurrence frequency derived by the CM-SAF and ISCCP-like methods shows a strong peak from 11:12 to 12:12 UTC. This could be due to a backscatter geometry effect; azimuth difference angles in this period are 160° - 180° . Since the LUT reflectances are less accurate for these unfavorable backscatter viewing geometries, for the CM-SAF method the increased 0.6- and 1.6- μm reflectance may lead to more water retrievals. For the ISCCP-like method, increased 0.6- μm reflectance leads to a smaller emissivity correction (see Equations 2 and 3), which in turn leads to a higher cloud-top temperature. After local noon (varying from 13:37-13:47 CEST), water (ice) occurrence gradually decreases (increases). This change in water and ice occurrence over the day is reproduced well by all methods, although some bias remains ($\sim 10\%$), mainly for the water cloud occurrence frequency. Further, the increase in ice cloud occurrence frequency after 13:12 CEST is reproduced with a small lag by the satellite methods, this could be due to the difference in resolution between ground and satellite measurements.

The correlation coefficients as obtained from the 15-minute binned observations are presented in Table 4. Correlation is significant for all methods for both the water and ice occurrence frequency. Since the original dataset was small ($n=48$), a bootstrap technique was used to assess the

reliability of the obtained correlations. The standard deviation of the bootstrapped correlations is assumed to indicate the error of the original correlation r_0 . For the 15-minute data, all r_0 -values are within one standard deviation, which means that the correlation is reliable. For both the diurnal cycle of water and ice cloud occurrence frequency, the MODIS-like method shows best performance with correlations of 0.89 and 0.86 for water and ice, respectively. The ISCCP-like and CM-SAF method have values between 0.67 and 0.76. The above values show significant skill for the number of data points used.

[Table 4 about here.]

5. Conclusions

In this paper, three cloud phase determination methods have been evaluated for their use in climate monitoring applications in midlatitude coastal climate. The methods investigated are a MODIS-like thermal infrared method, an ISCCP-like method, and a method developed within the framework of the CM-SAF. Using one year of SEVIRI data (May 2004-April 2005), retrievals of the methods were compared to collocated ground-based cloud phase retrievals from cloud radar and lidar data at Cabauw, The Netherlands. Three quality aspects of the satellite retrievals were evaluated: 1) instantaneous cloud phase retrievals, 2) monthly averaged water and ice cloud occurrence frequency, and 3) diurnal cycle of cloud phase for May-August 2004.

The ground-based algorithm (Illingworth and Coauthors 2007) used in this research retrieves cloud phase information on a very high temporal resolution with a vertical range of ~ 12 km. This in contrast to satellite imagery, which mostly derives cloud phase information from the uppermost part of a cloud. To account for these differences, ground-based cloud phase retrievals

were collected over 30-minute time windows. Furthermore, in order to obtain a straightforward comparison of satellite to ground-based derived cloud phase retrievals, the 30-minute averaged thickness of water, ice, and mixed phase layers was considered to label each time window period with a unique phase. Using the ground-based cloud phase dataset, it was shown that ice cloud occurrence frequency has a maximum during the summer ($\sim 40\%$), probably due to convection, and a minimum during winter ($\sim 15\%$). The ground-based water cloud occurrence frequency peaks in November 2004 ($\sim 30\%$). The fraction of mixed phase clouds gradually increases from 30% to $\sim 60\%$ towards the winter season, which could be related to synoptic-scale weather systems dominating the western European climate during winter. These systems contain substantial amounts of supercooled water clouds (Naud et al. 2006; Rauber and Tokay 1991).

All methods show small instantaneous bias for thick water and ice clouds with values within 5%. The ISCCP-like method has a larger bias for pure water clouds ($\sim 10\%$), which is likely due to the 260 K threshold leading to misdetection of water clouds existing at lower temperatures. Hogan et al. (2003) found that $\sim 25\%$ of ground-based lidar observed clouds at Chilbolton (United Kingdom) with temperatures lower than 258 K contain supercooled water layers.

For the dataset investigated, all methods show high precision in retrieving the water and ice cloud occurrence frequency during summer, with URMSE values mostly within 5%, and decreases during the winter months to 10-15%. The CM-SAF method is best capable of reproducing the annual cycle, mainly for the water cloud occurrence frequency, for which an almost constant positive bias of $\sim 8\%$ was found. This is largely coupled to the more direct observation of cloud phase due to the usage of visible and near-infrared reflectance. However, since this method can only be used during daytime, additional thermal infrared channel radiances are still required to obtain full day coverage. The ISCCP- and MODIS-like methods reproduce the annual cycle accu-

rately during the summer, but less clearly during the winter months. For the ISCCP-like method this is probably connected to the indirect relation of cloud phase to cloud-top temperature. Especially during the winter months when clouds are more stratiform and are more likely to contain supercooled liquid water at temperatures <260 K, a considerable amount of water clouds may be misclassified. The usage of dynamical temperature thresholds depending on e.g. the cloud dynamics can improve the accuracy for detection of the monthly variability of cloud phase.

For May-August 2004, all methods are well capable of reproducing the diurnal cycle of water and ice cloud occurrence. It was found that the MODIS-like method reproduces this cycle best, with correlations of 0.86 and 0.89 for the diurnal water and ice cloud occurrence frequency, respectively. CM-SAF and ISCCP-like methods have lower (~ 0.7), but still significant, correlation coefficients. The lower correlations compared to the MODIS-like method are likely linked to a lower signal-to-noise ratio and the usage of a temperature threshold for the CM-SAF and ISCCP-like method, respectively.

It is stressed that the very promising results were obtained over a midlatitude coastal climate area using one year of data. In order to obtain a high-quality global cloud phase climatology and to evaluate the interannual variability of cloud phase, more research on cloud phase determination using SEVIRI data over different climate regions and longer time periods is required. Furthermore, accuracy of cloud phase determination needs also to be assessed for nighttime scenes. Finally, the development and evaluation of mixed phase cloud categorization will be required as these clouds make up a significant part ($\sim 40\%$ averaged over the year investigated as derived from the ground dataset used) of all clouds.

Acknowledgement

This work was performed within the EUMETSAT funded Climate Monitoring Satellite Application Facility (CM-SAF) project. We thank the CloudNET project team (European Union contract EVK2-2000-00611) for providing the target classification and cloud boundaries, which was produced by the University of Reading using measurements from the Cabauw Experimental Site for Atmospheric Research (CESAR). Dr. Jérôme Riédi (University of Lille, France) is acknowledged for making the SEVIRI cloudmask available. Furthermore, we thank Dr. Bryan Baum (University of Wisconsin, Madison, USA) for providing the code of the MODIS thermal infrared cloud phase detection method. Finally, we thank Prof. Bart van den Hurk (KNMI) for fruitful discussions on the manuscript.

References

- Arking, A. and J. D. Childs, 1985: Retrieval of cloud cover parameters from multispectral satellite images. *J. Climate Appl. Meteor.*, **24**, 322–333.
- Baum, B. A., P. F. Soulen, K. I. Strabala, M. D. King, S. A. Ackerman, W. P. Menzel, and P. Yang, 2000: Remote sensing of cloud properties using MODIS Airborne Simulator imagery during SUCCESS: 2. Cloud thermodynamic phase. *J. Geophys. Res.*, **105**, 11781–11792.
- Chepfer, H., P. Goloub, J. Spinhirne, P. H. Flamant, M. Lavorato, L. Sauvage, G. Brogniez, and J. Pelon, 2000: Cirrus cloud properties derived from POLDER-1/ADEOS polarized radiances: First validation using a ground-based lidar network. *J. Appl. Meteor.*, **39**, 154–168.
- De Haan, J. F., P. B. Bosma, and J. W. Hovenier, 1987: The adding method for multiple scattering calculations of polarized light. *Astron. & Astrophys.*, **183**, 371–391.
- Doelling, D. R., L. Nguyen, and P. Minnis, 2004: Calibration comparisons between SEVIRI, MODIS and GOES data. *Proc. 2004 EUMETSAT Meteor. Satellite Conf., Prague, Czechian Republic*, 77–83.
- Downing, H. D. and D. Williams, 1975: Optical constants of water in the infrared. *J. Geophys. Res.*, **80**, 1656–1661.
- Efron, B. and R. J. Tibshirani, 1993: *An introduction to the bootstrap*. CRC Press Online, 436 pp.
- EUMETSAT, 2007: A planned change to the MSG Level 1.5 Image Production Radiance Definition. Scientific report, EUM/OPS-MSG/TEN/06/0519.

- Hansen, J. E. and J. B. Pollack, 1970: Near-infrared light scattering by terrestrial clouds. *J. Atmos. Sci.*, **27**, 265–281.
- Hansen, J. E. and L. D. Travis, 1974: Light scattering in planetary atmospheres. *Space Sci. Rev.*, **16**, 527–610.
- Hess, M. and M. Wiegner, 1994: COP: a data library of optical properties of hexagonal ice crystals. *Appl. Opt.*, **33**, 7740–7746.
- Hogan, R. J., A. J. Illingworth, J. P. V. Poiares-Baptista, and E. J. O’Connor, 2003: Characteristics of mixed-phase clouds, part II: A climatology from ground-based lidar. *Quart. J. Roy. Meteor. Soc.*, **129**, 2117–2134.
- Illingworth, A. J. and Coauthors, 2007: Continuous evaluation of cloud profiles in seven operational models using ground-based observations. *Bull. Amer. Meteor. Soc.*, **88**, 883–898.
- Jolivet, D. and A. J. Feijt, 2005: Quantification of the accuracy of LWP fields derived from NOAA - 16 Advanced Very High Resolution Radiometer over three ground stations using microwave radiometers. *J. Geophys. Res.*, **110**, D11204, doi:10.1029/2004JD005205.
- Knap, W. H., P. Stammes, and R. B. A. Koelemeijer, 2002: Cloud thermodynamic phase determination from near-infrared spectra of reflected sunlight. *J. Atmos. Sci.*, **59**, 83–96.
- Loeb, N. G. and J. A. Coakley, 1998: Inference of marine stratus cloud optical depths from satellite measurements: does 1D theory apply? *J. Climate*, **11**, 215–233.
- Minnis, P., D. P. Garber, D. F. Young, R. F. Arduini, and Y. Takano, 1998: Parameterizations of

- reflectance and effective emittance for satellite remote sensing of cloud properties. *J. Atmos. Sci.*, **55**, 3313–3339.
- Mittermaier, M. P. and A. J. Illingworth, 2003: Comparison of model-derived and radar-observed freezing-level heights: Implications for vertical reflectivity profile-correction schemes. *Quart. J. Roy. Meteor. Soc.*, **129**, 83–95.
- Nakajima, T. and M. D. King, 1990: Determination of the optical thickness and effective particle radius of clouds from reflected solar radiation measurements, part 1: Theory. *J. Atmos. Sci.*, **47**, 1878–1893.
- Naud, C. M., A. D. Del Genio, and M. Bauer, 2006: Observational constraints on the cloud thermodynamic phase in midlatitude storms. *J. Climate*, **19**, 5273–5288.
- Pilewskie, P. and S. Twomey, 1987: Discrimination of ice from water clouds by optical remote sensing. *Atmos. Res.*, **21**, 113–122.
- Platnick, S. E., M. D. King, S. A. Ackerman, W. P. Menzel, B. A. Baum, J. C. Riédi, and R. A. Frey, 2003: The MODIS cloud products: Algorithms and examples from Terra. *IEEE Geosci. Remote Sens.*, **41**, 459–473.
- Pruppacher, H. R. and J. D. Klett, 1997: *Microphysics of Clouds and Precipitation, 2nd rev. and enl. ed.*. Kluwer Academic Publishers, 954 pp.
- Rauber, R. M. and A. Tokay, 1991: An explanation for the existence of supercooled water at the top of cold clouds. *J. Atmos. Sci.*, **48**, 1005–1023.

- Riédi, J. C., P. Goloub, and R. T. Marchand, 2001: Comparison of POLDER cloud phase retrievals to active remote sensor measurements at the ARM SGP site. *Geophys. Res. Lett.*, **28**, 2185–2188.
- Roebeling, R. A., A. J. Feijt, and P. Stammes, 2006a: Cloud property retrievals for climate monitoring: Implications of differences between Spinning Enhanced Visible and Infrared Imager (SEVIRI) on METEOSAT-8 and Advanced Very High Resolution Radiometer (AVHRR) on NOAA-17. *J. Geophys. Res.*, **111**, doi:10.1029/2005JD006990.
- Roebeling, R. A., N. A. J. Schutgens, and A. J. Feijt, 2006b: Analysis of uncertainties in SEVIRI cloud property retrievals for climate monitoring. *12th conference on Atmospheric Radiation*, Am. Meteor. Soc., Madison, WI, CD-ROM, P4.51.
- Rossow, W. B. and R. A. Schiffer, 1999: Advances in understanding clouds from ISCCP. *Bull. Amer. Meteor. Soc.*, **80**, 2261–2287.
- Stammes, P., 2001: Spectral radiance modelling in the UV-Visible range. *IRS 2000: Current problems in Atmospheric Radiation*, W. L. Smith and Y. M. Timofeyev, eds., A. Deepak, Hampton, VA, 385–388.
- Strabala, K. I., S. A. Ackerman, and W. P. Menzel, 1994: Cloud properties inferred from 8-12 μm data. *J. Appl. Meteor.*, **33**, 212–229.
- Turner, D. D., 2005: Arctic mixed-phase cloud properties from AERI lidar observations: algorithm and results from SHEBA. *J. Appl. Meteor.*, **44**, 427–444.
- Turner, D. D., S. A. Ackerman, B. A. Baum, P. E. Rivercombe, and P. Yang, 2003: Cloud phase

determination using ground-based AERI observations at SHEBA. *J. Appl. Meteor.*, **42**, 701–715.

Warren, S. G., 1984: Optical constants of ice from the ultraviolet to the microwave. *Appl. Opt.*, **23**, 1206–1225.

List of Tables

1	Thresholds for the MODIS thermal infrared cloud phase determination method using MODIS (left column) and SEVIRI data (right column). BTD refers to brightness temperature difference 8.5-11.0 μm and 8.7-10.8 μm for MODIS and SEVIRI, respectively.	37
2	Criteria applied to 30-minute averages of ground-based observed water, ice, and mixed cloud layer thickness for calculation of monthly averaged cloud phase occurrence. Δh_i refers to ice layer thickness, Δh_w to water layer thickness, and Δh_m to mixed layer thickness.	38
3	Weighted correlation coefficients (r_0) and median bootstrap correlation (r_b) with standard deviation between satellite and ground-based derived water and ice cloud occurrence frequency for May 2004-April 2005.	39
4	Correlation coefficients between the satellite and ground-based derived diurnal cycle of water and ice cloud occurrence frequency for May-August 2004. r_0 represents the correlation using 15-minute binning of the original dataset ($n=48$), r_b denotes the median bootstrap correlation with the standard deviation.	40

Table 1: Thresholds for the MODIS thermal infrared cloud phase determination method using MODIS (left column) and SEVIRI data (right column). BTD refers to brightness temperature difference 8.5-11.0 μm and 8.7-10.8 μm for MODIS and SEVIRI, respectively.

phase	MODIS	SEVIRI
water	$BT > 238 \text{ K} \ \& \ BTD < -1.0$ or $BT \geq 285 \text{ K} \ \& \ BTD \leq -0.5 \text{ K}$	$BT > 238 \text{ K} \ \& \ BTD < -0.5$ or $BT \geq 285 \text{ K} \ \& \ BTD \leq 0.0 \text{ K}$
ice	$BT \leq 238 \text{ K} \ \& \ BTD > 1.0 \text{ K}$	$BT \leq 238 \text{ K} \ \& \ BTD > 1.5 \text{ K}$
mixed	$BT > 238 \text{ K} \ \& \ BT < 268 \text{ K} \ \& \ -0.25 \text{ K} \leq BTD < 0.5 \text{ K}$	$BT > 238 \text{ K} \ \& \ BT < 268 \text{ K} \ \& \ 0.25 \text{ K} \leq BTD < 1.0 \text{ K}$
undefined	$238 \text{ K} < BT < 268 \text{ K} \ \& \ -1.0 \text{ K} < BTD < -0.25 \text{ K}$	$238 \text{ K} < BT < 268 \text{ K} \ \& \ -0.5 \text{ K} < BTD < 0.25 \text{ K}$

Table 2: Criteria applied to 30-minute averages of ground-based observed water, ice, and mixed cloud layer thickness for calculation of monthly averaged cloud phase occurrence. Δh_i refers to ice layer thickness, Δh_w to water layer thickness, and Δh_m to mixed layer thickness.

cloud phase	criterion
ice	$\Delta h_i > 2500$ m
water	$\Delta h_i < 600$ m & $(\Delta h_w / \Delta h_m) > 4$
mixed phase	0 m < $\Delta h_i < 2500$ m & $(\Delta h_w / \Delta h_m) < 4$

Table 3: Weighted correlation coefficients (r_0) and median bootstrap correlation (r_b) with standard deviation between satellite and ground-based derived water and ice cloud occurrence frequency for May 2004-April 2005.

method	$r_{0,\text{water}}$	$r_{b,\text{water}}$	$r_{0,\text{ice}}$	$r_{b,\text{ice}}$
CM-SAF	0.94	0.93 ± 0.02	0.98	0.93 ± 0.02
ISCCP-like	0.92	0.91 ± 0.03	0.97	0.91 ± 0.03
MODIS-like	0.92	0.91 ± 0.03	0.97	0.91 ± 0.03

Table 4: Correlation coefficients between the satellite and ground-based derived diurnal cycle of water and ice cloud occurrence frequency for May-August 2004. r_0 represents the correlation using 15-minute binning of the original dataset ($n=48$), r_b denotes the median bootstrap correlation with the standard deviation.

	$r_{0,\text{water}}$	$r_{b,\text{water}}$	$r_{0,\text{ice}}$	$r_{b,\text{ice}}$
CM-SAF	0.73	0.74 ± 0.06	0.67	0.67 ± 0.09
ISCCP-like	0.76	0.76 ± 0.07	0.70	0.70 ± 0.07
MODIS-like	0.89	0.89 ± 0.03	0.86	0.87 ± 0.04

List of Figures

- 1 Imaginary index of refraction for water (solid) and ice (dashed) between 8 and 13 μm . Water indices are from Downing and Williams (1975), ice indices are from Warren (1984). 43
- 2 Modeled 0.6 and 1.6 μm reflectances for $\theta_o=20^\circ$, $\theta=28^\circ$, and $\phi-\phi_o=100^\circ$. Cloud optical thickness is denoted by various vertically oriented lines, effective radius by horizontally oriented lines. Water particles are represented in the upper part of the graph, ice particles in the lower part. 44
- 3 Location of the Cabauw measurement site. 45
- 4 Bias between instantaneous satellite and ground-based cloud phase retrievals for water (grey) and ice (black). The x-axis values indicate the maximum and minimum ice layer thickness for ground-based observed water and ice clouds, respectively. The CM-SAF method is plotted solid, the ISCCP-like method dotted, and the MODIS-like method dashed. The histograms indicate the number of collocated observations with scaling on the right-hand axis. 46
- 5 Monthly averages of ground-based derived liquid water (dotted), ice (dashed), and mixed phase (solid) clouds using a three-month moving window. Clouds are labeled as ice for 30-minute average thickness >2500 m, water clouds contain <600 m of ice overhead (see also Table 2). The grey histogram indicates the number of valid observations for each three-month period. 47

6	(a,d) Monthly averaged liquid water and ice cloud occurrence frequency for the SEVIRI methods and ground-based method; (b,e) unbiased root-mean-square error (URMSE) for the SEVIRI methods; (c,f) liquid water and ice cloud occurrence frequency for the SEVIRI methods and ground-based method normalized by the respective yearly average. Liquid water cloud results are on the left, ice cloud results are on the right. Results were obtained using a three-month moving window.	48
7	Monthly weighted correlation coefficients based on daily averaged water (left panel) and ice (right panel) occurrence frequency using a three-month moving window for CM-SAF (dotted), ISCCP-like (dashed), and MODIS-like (dashed-dotted) methods.	49
8	Diurnal cycle of water (left panel) and ice (right panel) cloud occurrence frequency for SEVIRI methods versus ground-based observed values (solid line) for May-August 2004. Values are obtained from measurements binned over 1-hour periods from 6:12-18:12 UTC (8:12-20:12 Central European Summer Time). The number of observations in each bin is denoted by the grey histogram, with scaling on the right hand axis.	50

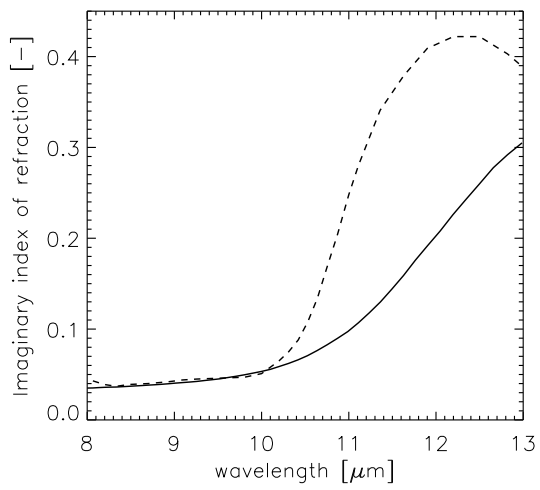


Figure 1: Imaginary index of refraction for water (solid) and ice (dashed) between 8 and 13 μm . Water indices are from Downing and Williams (1975), ice indices are from Warren (1984).

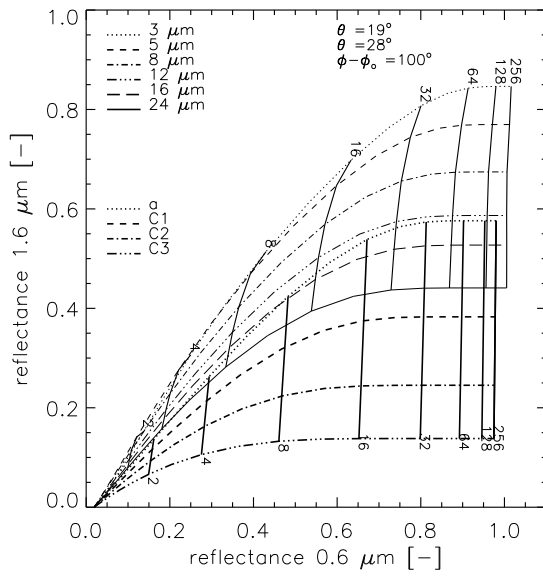


Figure 2: Modeled 0.6 and 1.6 μm reflectances for $\theta_0=20^\circ$, $\theta=28^\circ$, and $\phi-\phi_0=100^\circ$. Cloud optical thickness is denoted by various vertically oriented lines, effective radius by horizontally oriented lines. Water particles are represented in the upper part of the graph, ice particles in the lower part.

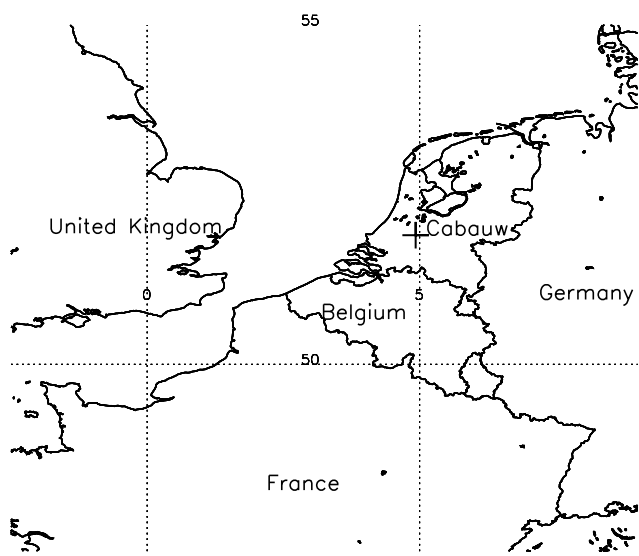


Figure 3: Location of the Cabauw measurement site.

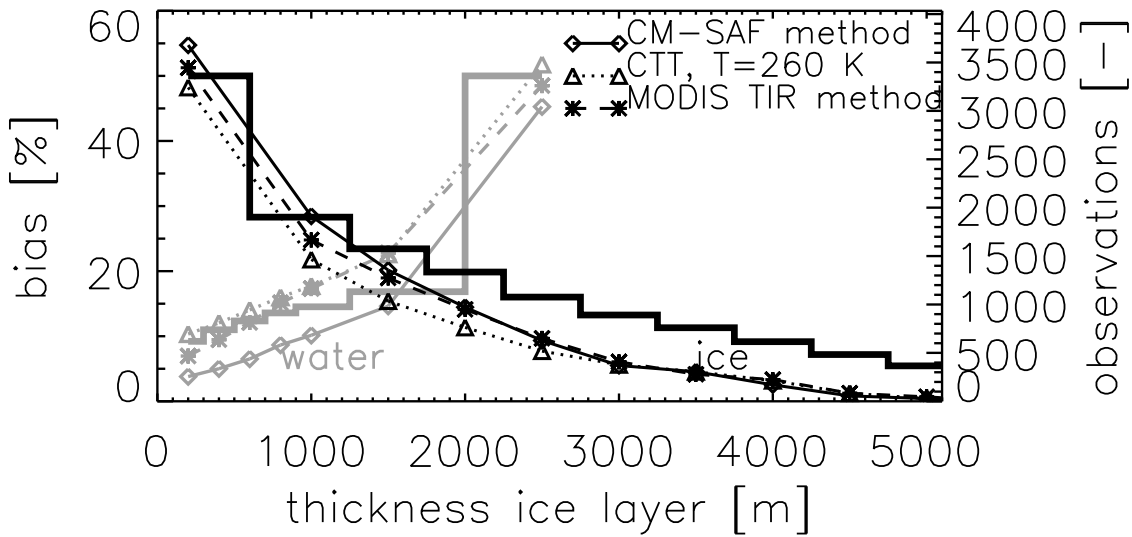


Figure 4: Bias between instantaneous satellite and ground-based cloud phase retrievals for water (grey) and ice (black). The x-axis values indicate the maximum and minimum ice layer thickness for ground-based observed water and ice clouds, respectively. The CM-SAF method is plotted solid, the ISCCP-like method dotted, and the MODIS-like method dashed. The histograms indicate the number of collocated observations with scaling on the right-hand axis.

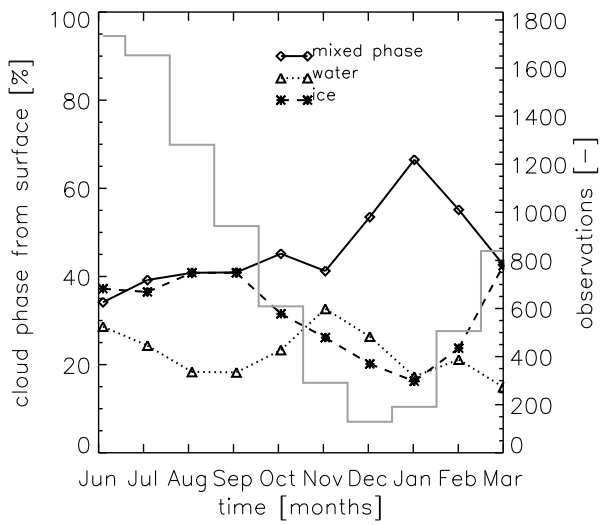


Figure 5: Monthly averages of ground-based derived liquid water (dotted), ice (dashed), and mixed phase (solid) clouds using a three-month moving window. Clouds are labeled as ice for 30-minute average thickness >2500 m, water clouds contain <600 m of ice overhead (see also Table 2). The grey histogram indicates the number of valid observations for each three-month period.

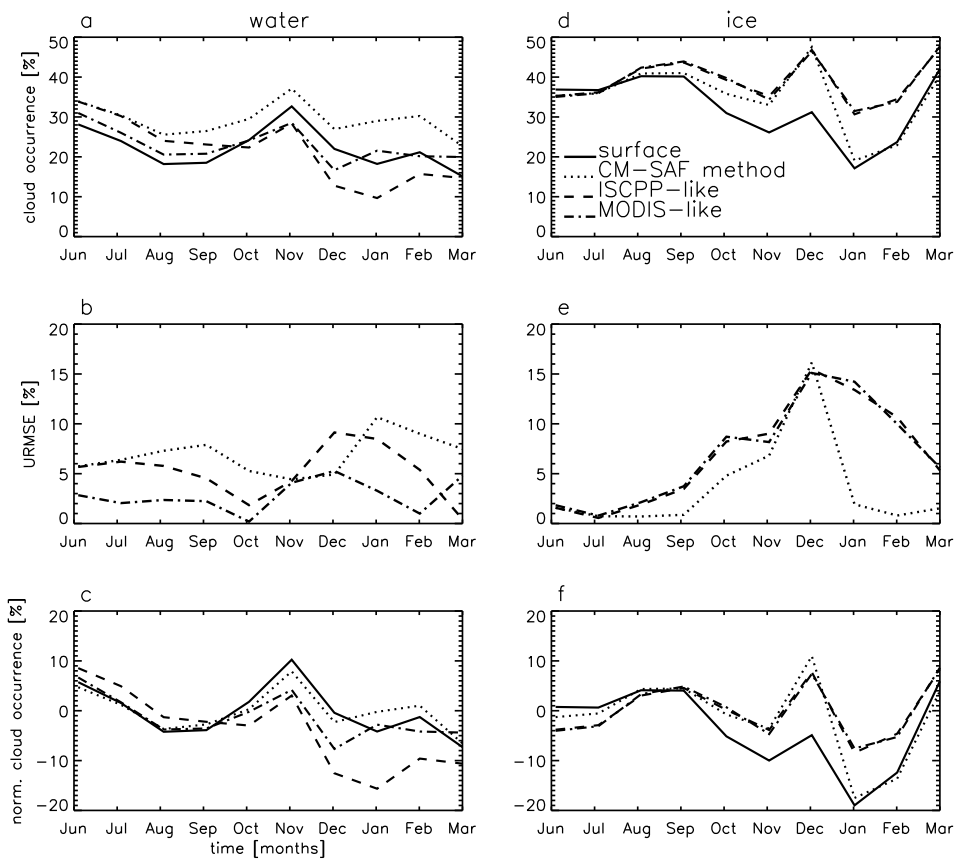


Figure 6: (a,d) Monthly averaged liquid water and ice cloud occurrence frequency for the SEVIRI methods and ground-based method; (b,e) unbiased root-mean-square error (URMSE) for the SEVIRI methods; (c,f) liquid water and ice cloud occurrence frequency for the SEVIRI methods and ground-based method normalized by the respective yearly average. Liquid water cloud results are on the left, ice cloud results are on the right. Results were obtained using a three-month moving window.

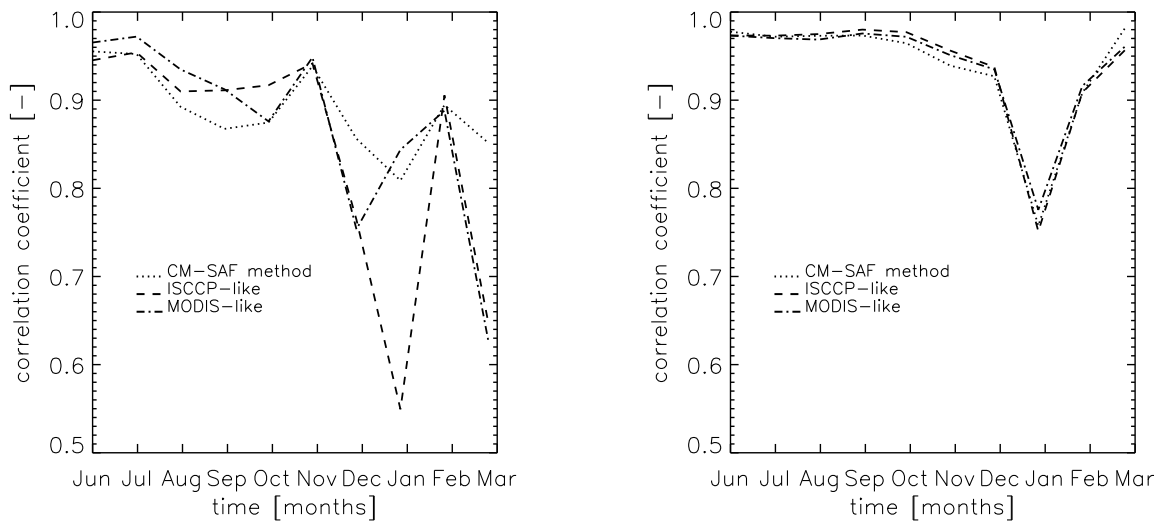


Figure 7: Monthly weighted correlation coefficients based on daily averaged water (left panel) and ice (right panel) occurrence frequency using a three-month moving window for CM-SAF (dotted), ISCCP-like (dashed), and MODIS-like (dashed-dotted) methods.

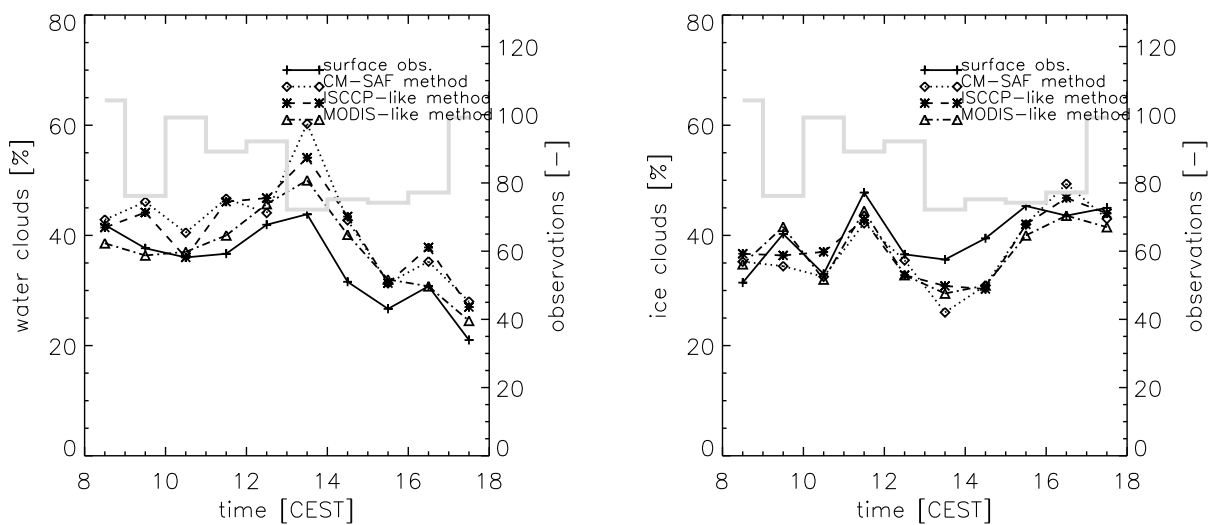


Figure 8: Diurnal cycle of water (left panel) and ice (right panel) cloud occurrence frequency for SEVIRI methods versus ground-based observed values (solid line) for May-August 2004. Values are obtained from measurements binned over 1-hour periods from 6:12-18:12 UTC (8:12-20:12 Central European Summer Time). The number of observations in each bin is denoted by the grey histogram, with scaling on the right hand axis.